CHEMISTRY OF MATERIALS

Article

pubs.acs.org/cm

Fabrication of Metallic Nanomesh: Pt Nano-Mesh as a Proof of Concept for Stretchable and Transparent Electrodes

Ho Young Jang,[†] Seoung-Ki Lee,[‡] Sang Hyun Cho,[†] Jong-Hyun Ahn,*[,∥] and Sungho Park*[,†,§]

[†]Department of Energy Science, [‡]School of Advanced Materials Science and Engineering, and [§]Department of Chemistry, BK21 School of Chemical Materials Science, Sungkyunkwan University, Suwon 440-746, South Korea

[∥]School of Electrical & Electronic Engineering, Yonsei University, Seoul 120-749, South Korea

ABSTRACT: Two-dimensional ordered arrays of honeycomb morphology of platinum are fabricated by using anodized aluminum oxide template and metal sputtering methods. The resulting metal films are highly conductible (71 Ω/sq), stretchable (16.8%), and transparent (75.2% at 550 nm). The presented synthetic strategy is scalable to large area without noticeable defects by incorporating the deposition of a thin layer of silver. In addition, both the pore size and wall thickness of platinum nanomesh films are straightforwardly controlled with sputtering time. As a proof of concept, the metal nanomesh films using AAO template suggest a new concept of synthesizing transparent and stretchable metal electrodes for future electronic devices.

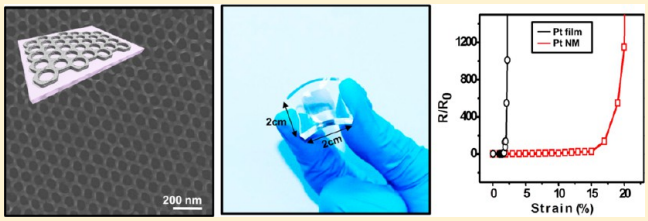

KEYWORDS: *nanomesh, AAO, stretchable electrode, transparent electrode, honeycomb*

■ INTRODUCTION

One fundamental goal of modern nanochemistry involves developing various synthetic pathways to unprecedented nanostructures in order to tailor their physical and chemical properties.[1−4] Morphological tunability on a nanometer scale allows one to change the original properties of the bulk component. One representative example in this category is graphene.[5−7] Graphene has gained much attention because of its significant potential for application in electronics[8−10] but cannot yet be utilized for highly effective field-effect transistors due to its zero bandgap properties.[11,12] However, it is well-known that the processing of graphene sheets into two-dimensional nanoribbons with widths of less than 10 nm can lead to bandgap opening, which is totally different from the properties of the original graphene sheets.[13−15] Simple variation in morphology can endow new material properties to the original counterpart. Herein, we demonstrate the synthetic strategy leading to metallic nanomesh architecture by using an anodized aluminum oxide (AAO) template and metal sputtering. The resulting metal nanomesh could be transferred to polymer substrates and exhibit good transparency normal to the *xy* plane of the substrate, while keeping good electrical conductivity through the *xy* plane. Transparent conducting electrodes are crucial components in many optoelectronic devices, including solar cells. In order to replace indium tin oxide (ITO) electrodes, there are many reports that describe new types of transparent electrodes such as macroscopic metallic grids, solution-processed random metal nanowire networks, and graphene.[16−20] Our metal nanomesh exhibited comparable transparency to the aforementioned examples and could be easily transferred to a solid substrate like glass, silicon wafer, or polymer. Noticeable advantages of metal nanomesh reported herein are the straightforward controllability of bridge width, a good periodic array of nanoholes, and versatile transfer to various solid substrate types. As compared to a continuous bulk metal film, the 2-D metal nanomesh is expected to be more tolerable to the mechanical strain that is induced by biaxial stretching. In open mesh geometries, strains applied in the plane of the substrate are expected to be accommodated by in-plane rotations, with a motion similar to that of scissors.[21] Macroscopically, this concept has been proven in metal mesh architecture.[21] Tensile strains applied at the ends of a narrow strip with open mesh cause the bridge to rotate in a manner that transforms the open squares into distorted rhombuses.[21] We expect that a similar mechanical distortion would accommodate the tensile strains if the metal film has a 2-D nanomesh architecture. Therefore, it would be possible to fabricate a transparent and stretchable metallic electrode by incorporating open nanomeshes into the bulk metal film.

■ EXPERIMENTAL SECTION

An AAO template was prepared according to the method reported in the literature.[22] Typical AAO templates showed a pore diameter of 80 (±5) nm, and we used this template for the formation of Pt nanomesh. A layer of Pt was deposited using an Ar plasma sputter coater (Cressington 108 auto) while varying time range from 40 to 60 s with a current level of 30 mA. Pore sizes are 11, 22, and 30 nm, while the corresponding standard deviations are 2, 3, and 2 nm, respectively. Then, a Poly (methyl methacrylate) (PMMA) coating layer was formed using a PMMA solution dissolved in dichlorobenzene (MICRO CHEM 950 PMMA C 4) with a spin-coater (Dong Ah

Received: June 27, 2013
Revised: August 5, 2013
Published: August 7, 2013

Tech & Trade Corp. ACE-200), operated at 3000 rpm for 1 min. Ar plasma sputter was used to deposit a 200 nm thick Ag layer for 300 s under an applied current of 40 mA. AAO templates were completely dissolved by 3 M NaOH solution, washed repeatedly with DI water, and then transferred onto a DI water surface at room temperature. The samples were transferred onto clean substrates (SiO_2 wafer or glass substrates) and dried in an 80 °C oven. The Ag layer was dissolved using 60% HNO_3 solution in 5 min and washed repeatedly with DI water. The PMMA layer was dissolved by acetone in 30 min, leading to the pure Pt nanomesh on the substrates.

Characterizations: FESEM (JEOL 7600F) was used to observe the morphological and structural properties of the Pt nanomesh structure pore size. Transmittance spectra of Pt nanomesh and film were measured by a UV−vis spectrometer (Scinco S-3100). AFM (Veeco 840-012-711) was used to analyze cross-sectional profiles of the Pt nanomesh structure. *I*−*V* measurement and stretching of Pt nanomesh structure were measured by a semiconductor analyzer (KEITHLEY 4200-SCS).

RESULTS AND DISCUSSION

The synthetic routes of metallic nanomesh are illustrated in Figure 1. We employ AAO templates and metal sputtering

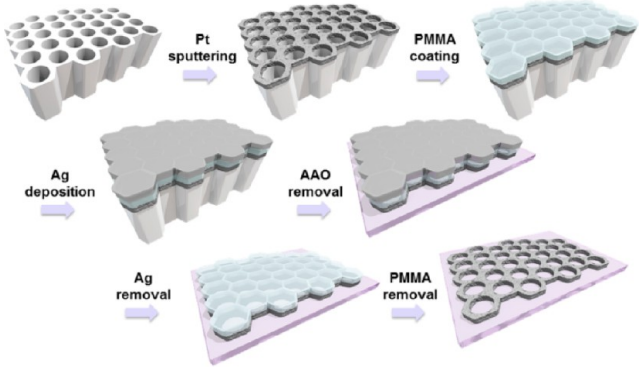

Figure 1. Schematic representation of synthesis of Pt nanomesh structure.

methods. In particular, the AAO templates allow one to fabricate large, ordered, and tunable 2D metal nanomesh networks because they are scalable, and additionally, their pore size and periodicity can be easily modulated. In a typical experiment, a thin layer (~30 nm) of Pt is sputtered on one side of the AAO templates. Then, a PMMA adlayer is formed on top of the Pt via spin-coating method. The resulting samples are dried under air and then transferred to a Ag sputtering chamber where a thin layer (~200 nm) of Ag is deposited on top of the PMMA. The Ag layer coating on top of the PMMA turned out to be critical to generate a large area of metal nanomesh without defects. As demonstrated in Figure 2, the metal nanomesh without Ag layer deposition contained many significant macroscopic defects, such as void spaces and breakage of metal linkages. Obviously, such an imperfect metal nanomesh film will exhibit poor conductivity due to a lack of sufficient current flow channels through the plane of substrates. In contrast, the resulting metal nanomesh synthesized using Ag layer deposition shows a well-ordered nanomesh without any noticeable defect. The image shows the excellent uniformity of the network over a large area. All of the bridges are well connected, and there is no noticeable void space over the entire metal nanomesh. The formation of a Ag layer on the PMMA surface prevents the curling of samples and the loss of PMMA during the dissolution of AAO with 3 M

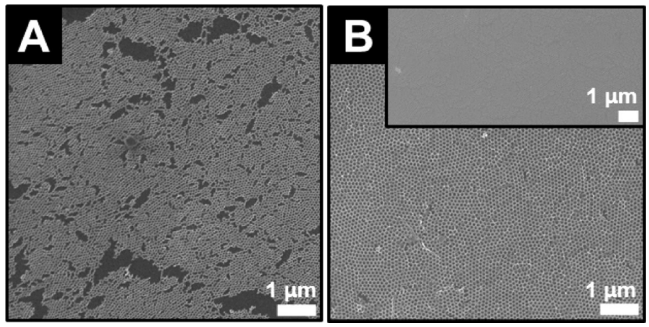

Figure 2. SEM images of Pt nanomesh structure films without Ag deposition process (A) and with Ag deposition process (B). Inset shows the larger image of panel (B).

NaOH solution. The floating metal nanomesh can be transferred to any solid substrate at this step. Subsequently, the Ag layer is dissolved by HNO_3 solution, and then the PMMA adlayer is removed by acetone. The morphology of each sample is investigated by field-emission scanning electron microscopy (FESEM) as shown in Figure 3. Pt is deposited on

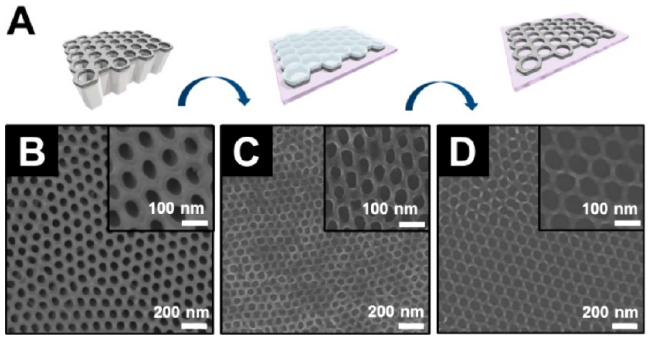

Figure 3. Fabrication process of Pt nanomesh structure film (A) with each corresponding SEM image (B−D).

the center part of AAO bridges without filling the nanochannels (panel B, Figure 3). The final Pt nanomesh is a replica of the AAO and exhibits good nanohole periodicity. We tested further to determine if we can tune the bridge width of the nanomesh by controlling the sputtering time (Figure 4). When we sputtered Pt under 30 mA, 40 s conditions, the resulting nanomesh shows a bridge width of 11 ± 2 nm, as well as a nearly monodisperse size distribution. Figure 4D−F displays the distribution of bridge widths. It is noteworthy that the smallest bridge width is not limited to 11 ± 2 nm, and it can go down below 10 nm. In contrast, when the sputtering condition changed to 30 mA, 50 s, the bridge width increased to 22 ± 3 nm and could be further increased up to 30 ± 2 nm while keeping a monodisperse size distribution (panels B and C, respectively). The corresponding optical image of Pt metal nanomesh transferred onto glass substrates is displayed in Figure 6A. As the bridge width increases, the dark feature of nanomesh becomes more noticeable. The comparable Pt bulk film with a thickness of 22 nm shows a transmittance of about 70% over the investigated spectral window (from 400 to 700 nm) without any noticeable spectral feature (blue dashed traces, Figure 5A). In contrast to Au or Ag, nanosized Pt shows no distinct surface plasmon resonance over the visible spectral window. All of the Pt nanomesh samples show featureless flat profiles similar to the spectrum of the bulk Pt film. Pt

dx.doi.org/10.1021/cm402085k | *Chem. Mater.* 2013, 25, 3535−3538

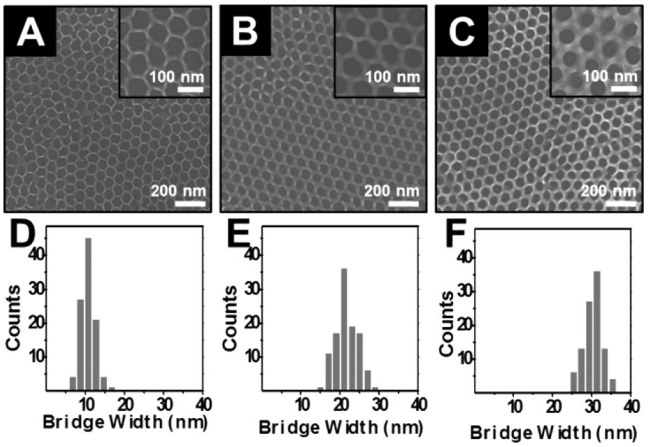

Figure 4. SEM images of Pt nanomesh structure films with various bridge widths in sputtering time of 40 s (A), 50 s (B), and 60 s (C) with current level of 30 mA. Inset figures show the high magnification SEM images of nanomesh structure films. Graphs are bridge-width distribution of nanomesh structure films calculated from parts A–C (D–F).

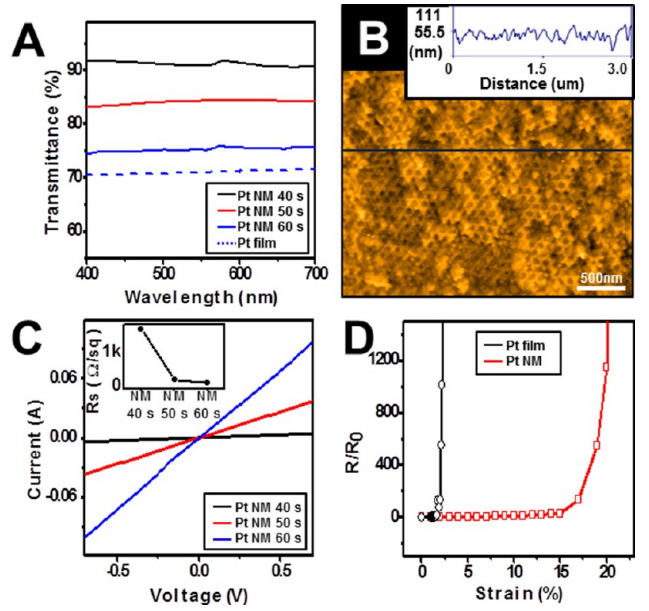

Figure 5. (A) Optical transmittance of Pt nanomesh structure films in 40 s, 50 s, and 60 s and platinum film deposited at the same amount of nanomesh structure film in 60 s with current level of 30 mA. (B) AFM image of Pt nanomesh structure film deposited with 30 mA for 60 s (solid blue line in part A) on Si substrate. Inset: Height profile along the solid lines. (C) $I-V$ characteristics for Pt nanomesh structure films at ambient condition (electrode gap width is 60 μm). (D) Change in resistance (R/R_0, where R_0 is the initial resistance at zero strain) of Pt film and nanomesh structure film transferred on PDMS substrate stretched toward the xy plane by ~25%.

nanomesh with a bridge width of 11 nm displays a very high transmittance of greater than 90% over the entire spectral window (black traces). As the bridge width increases, the transmittance decreases accordingly because the nanohole void portion decreases. The homogeneity of the nanomesh height profile was investigated with atomic force microscopy (AFM), which showed a rms roughness of ca. 22 nm. The height profile homogeneity is well represented in the inset of Figure 5B, which is measured along the blue solid line of Figure 5A. The electrical conductivity in the xy plane has been examined by forming a two-point contact at the end of the Pt nanomesh. The distance between two electrical contacts is about 60 μm, and the $I-V$ curves are measured by applying −0.7 V to one end and higher voltage (up to 0.7 V) to the other end, as shown in Figure 5C. The calculated sheet resistance values from resistance for each sample are 1667 Ω/sq, 185 Ω/sq, and 71 Ω/sq for Pt nanomesh for 40 s, 50 s, and 60 s with current level of 30 mA, respectively (Figure 5C, inset).[23] This value is comparable with other transparent electrodes.[16,24−26] Obviously, a thicker Pt nanomesh film displays better electrical conduction but diminished optical transmission, as represented in Figure 5A&C. Of central interest is the resistance variation when the Pt nanomesh films are parallel stretched. The photographs of the stretching experimental setup are displayed in Figure 6C&D, which correspond to before and after

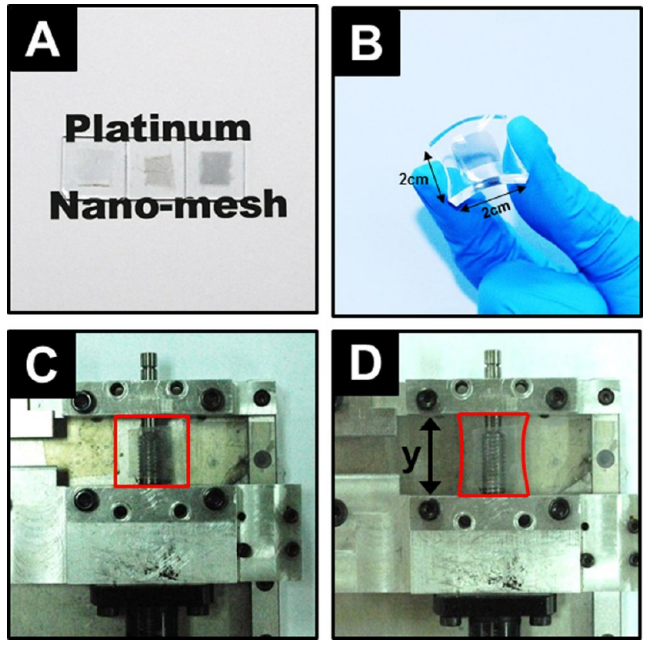

Figure 6. (A) Photograph image of Pt nanomesh structure films. (B) Photograph image of Pt nanomesh structure film for 60 s deposited with current level of 30 mA on PDMS. View of the setup used to generate strain (C, D). The samples were strained to the y axis.

stretching, respectively. When the bulk Pt films (thickness ~ 22 nm) without nanomesh patterns are stretched in the y-axis, there is no change in the resistance value until a stretch ratio of 2.0% is reached (as depicted in panel D, Figure 5). However, electrical failure suddenly occurred at a stretch ratio of 2.3%, whereas the Pt nanomesh films retain their initial resistance until the stretch ratio reaches 16.8%. After maximum strain level (16.8%), the nanomesh starts to change resistance gradually due to plastic deformation of Pt, and then it finally shows breakdown entirely. The Pt nanomesh films show seven times higher tolerance than the bulk Pt films. In open mesh geometries, strains applied in the plane of the substrate are expected to be accommodated by in-plane rotations and distortion of nanomeshes. Tensile strains applied at the ends of Pt films with open meshes may cause the bridge to rotate in a manner that transforms the open holes into distorted oval frames.[27] We expect that the mechanical distortion would accommodate the tensile strains without breakage of Pt films. Macroscopically, this concept can be demonstrated by carrying

dx.doi.org/10.1021/cm402085k | Chem. Mater. 2013, 25, 3535−3538

out a similar experiment with aluminum foils (Figure 7). In the case of bulk Pt films, there is no other way to accommodate the

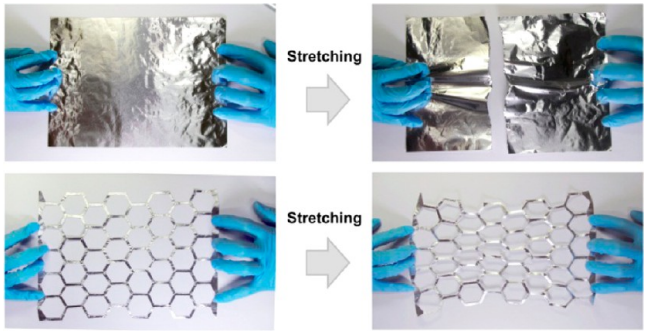

Figure 7. Photograph image of example test comparison between bulk film and mesh structure film.

applied tensile strains, and therefore cracks are formed at the threshold point of tensile strains. The accumulation of tensile strains on the cracks will eventually lead to the breakage of Pt bulk films.

■ CONCLUSION

In conclusion, the present results show that ultrathin Pt nanomesh films can be synthesized using an AAO template and metal sputtering methods. The resulting Pt nanomesh can be transferred to polymer substrates. We characterized the transmittance of visible light through the Pt nanomesh films and evaluated accommodation capability toward the stretching tensile strain in comparison to the bulk Pt counterpart. The open mesh architecture at a nanometer scale allowed the passage of light through the open nanoholes and could successfully prevent the film breakage due to in-plane rotations and distortion of nanomeshes. The presented metal architecture is scalable and can be fabricated with different metals. We expect a similar noble metal architecture will exhibit localized surface plasmon resonance and therefore can be utilized for various applications such as biosensors and optoelectronic devices.

■ AUTHOR INFORMATION

Corresponding Author

*E-mail: J.H. Ahn, ahnj@yonsei.ac.kr; S. Park, spark72@skku.edu.

Notes

The authors declare no competing financial interest.

■ ACKNOWLEDGMENTS

This work was supported by the National Research Foundation of Korea (National Leading Research Lab: 2012R1A2A1A03670370) and the Human Resources Development program (No. 20124010203270) of the Korea Institute of Energy Technology Evaluation and Planning (KETEP) grant funded by the Korea government Ministry of Knowledge Economy.

■ REFERENCES

(1) Jung, S.; Liu, L.; Shuford, K. L.; Park, S. *J. Phys. Chem. C* **2013**, *117* (6), 3141−3145.
(2) Lee, D.; Jang, H. Y.; Hong, S.; Park, S. *J. Colloid Interface Sci.* **2012**, *388*, 74−79.
(3) Lee, S. A.; Liu, L.; Kim, S. K.; Park, S. *J. Phys. Chem. C* **2012**, *116* (34), 18388−18393.
(4) Choi, Y.; Choi, J.-H.; Liu, L.; Oh, B.-K.; Park, S. *Chem. Mater.* **2013**, *25* (6), 919−926.
(5) Geim, A. K.; Novoselov, K. S. *Nat. Mater.* **2007**, *6* (3), 183−191.
(6) Kim, K. S.; Zhao, Y.; Jang, H.; Lee, S. Y.; Kim, J. M.; Kim, K. S.; Ahn, J.-H.; Kim, P.; Choi, J. Y.; Hong, B. H. *Nature* **2009**, *457* (7230), 706−710.
(7) Li, X. L.; Zhang, G. Y.; Bai, X. D.; Sun, X. M.; Wang, X. R.; Wang, E.; Dai, H. J. *Nat. Nanotechnol.* **2008**, *3* (9), 538−542.
(8) He, M.; Jung, J. H.; Qiu, F.; Lin, Z. Q. *J. Mater. Chem.* **2012**, *22* (46), 24254−24264.
(9) Huang, X.; Zeng, Z. Y.; Fan, Z. X.; Liu, J. Q.; Zhang, H. *Adv. Mater.* **2012**, *24* (45), 5979−6004.
(10) Wen, Z. H.; Wang, X. C.; Mao, S.; Bo, Z.; Kim, H.; Cui, S. M.; Lu, G. H.; Feng, X. L.; Chen, J. H. *Adv. Mater.* **2012**, *24* (41), 5610−5616.
(11) Meric, I.; Han, M. Y.; Young, A. F.; Ozyilmaz, B.; Kim, P.; Shepard, K. L. *Nat. Nanotechnol.* **2008**, *3* (11), 654−659.
(12) Novoselov, K. S.; Geim, A. K.; Morozov, S. V.; Jiang, D.; Katsnelson, M. I.; Grigorieva, I. V.; Dubonos, S. V.; Firsov, A. A. *Nature* **2005**, *438* (7065), 197−200.
(13) Jiao, L. Y.; Wang, X. R.; Diankov, G.; Wang, H. L.; Dai, H. J. *Nat. Nanotechnol.* **2010**, *5* (5), 321−325.
(14) Li, X. L.; Wang, X. R.; Zhang, L.; Lee, S. W.; Dai, H. J. *Science* **2008**, *319* (5867), 1229−1232.
(15) Pan, Z. H.; Liu, N.; Fu, L.; Liu, Z. F. *J. Am. Chem. Soc.* **2011**, *133* (44), 17578−17581.
(16) Li, X. S.; Zhu, Y. W.; Cai, W. W.; Borysiak, M.; Han, B. Y.; Chen, D.; Piner, R. D.; Colombo, L.; Ruoff, R. S. *Nano Lett.* **2009**, *9* (12), 4359−4363.
(17) Madaria, A. R.; Kumar, A.; Ishikawa, F. N.; Zhou, C. W. *Nano Res.* **2010**, *3* (8), 564−573.
(18) Rathmell, A. R.; Bergin, S. M.; Hua, Y. L.; Li, Z. Y.; Wiley, B. J. *Adv. Mater.* **2010**, *22* (32), 3558−+.
(19) Zhu, Y.; Sun, Z. Z.; Yan, Z.; Jin, Z.; Tour, J. M. *ACS Nano* **2011**, *5* (8), 6472−6479.
(20) Bae, S.; Kim, H.; Lee, Y.; Xu, X. F.; Park, J. S.; Zheng, Y.; Balakrishnan, J.; Lei, T.; Kim, H. R.; Song, Y. I.; Kim, Y. J.; Kim, K. S.; Ozyilmaz, B.; Ahn, J.-H.; Hong, B. H.; Iijima, S. *Nat. Nanotechnol.* **2010**, *5* (8), 574−578.
(21) Kim, D. H.; Rogers, J. A. *Adv. Mater.* **2008**, *20* (24), 4887−4892.
(22) Kim, S.; Shuford, K. L.; Bok, H. M.; Kim, S. K.; Park, S. *Nano Lett.* **2008**, *8* (3), 800−804.
(23) van de Groep, J. V.; Spinelli, P.; Polman, A. *Nano Lett.* **2012**, *12* (6), 3138−3144.
(24) Kim, K. K.; Reina, A.; Shi, Y. M.; Park, H.; Li, L. J.; Lee, Y. H.; Kong, J., Enhancing the conductivity of transparent graphene films via doping. *Nanotechnology* **2010**, *21*, (28).
(25) Hu, L. B.; Kim, H. S.; Lee, J. Y.; Peumans, P.; Cui, Y. *ACS Nano* **2010**, *4* (5), 2955−2963.
(26) Gunes, F.; Shin, H. J.; Biswas, C.; Han, G. H.; Kim, E. S.; Chae, S. J.; Choi, J. Y.; Lee, Y. H. *Acs Nano* **2010**, *4* (8), 4595−4600.
(27) Takahashi, T.; Takei, K.; Gillies, A. G.; Fearing, R. S.; Javey, A. *Nano Lett.* **2011**, *11* (12), 5408−5413.